RESEARCH ARTICLE

Editor's Choice

ADVANCED ELECTRONIC MATERIALS Open Access

www.advelectronicmat.de

Atomic Structure and Quasiparticle Interference of Epitaxial Graphene on Ferromagnetic Mn_5Ge_3

*Vivien Enenkel, Veronika Yastrebova, Elena Voloshina, Yuriy Dedkov, and Mikhail Fonin**

The implementation of graphene in spintronics requires the formation of high quality graphene–ferromagnet interfaces for efficient spin injection. By using low-temperature scanning tunneling microscopy (STM), the atomic structure as well as the electronic properties of epitaxial graphene/ferromagnetic -Mn_5Ge_3/semiconducting-Ge heterostructures are investigated. The formation of the graphene/Mn_5Ge_3 interface is performed by Mn evaporation on the graphene/Ge(110) surface combined with annealing during and after deposition, yielding graphene on Mn_5Ge_3 crystallites of two distinct types, each displaying a principal facet – graphene/Mn_5Ge_3(0001) and graphene/Mn_5Ge_3(11$\bar{2}$0). STM imaging shows graphene/Mn_5Ge_3 interfaces with a high degree of structural order down to the atomic level. The local electronic structure of graphene/Mn_5Ge_3 probed by d*I*/d*V* spectroscopy and by quasiparticle interference mapping is found to be very close to that of free-standing graphene, with only a very small electron doping. These findings provide important microscopic insights into a system with a potential for spintronics device fabrication compatible with modern semiconductor technology.

1. Introduction

Within the last two decades, graphene, a single layer of carbon atoms arranged in a honeycomb lattice, is the most studied 2D material owing to its fascinating properties as well as the device application perspectives.[1–6] Low intrinsic spin orbit interaction as well as low hyperfine interaction of the electron spins with the carbon nuclei, which in combination with high carrier mobility allow for excellent lateral spin transport, make graphene also a particularly promising material for spintronics.[7–12] The implementation of graphene in spintronic devices requires the realization of high-quality graphene/ferromagnet (graphene/FM) interfaces, whose spin-dependent properties strongly vary depending on the interaction between graphene and ferromagnet. Partially motivated by the theoretical works regarding the high spin-filtering efficiencies of graphene/FM interfaces,[13–15] early experimental studies focused on the investigation of epitaxial graphene/3*d*-FM systems, such as graphene/Ni(111)[16–19] and graphene/Co(0001).[20,21] Upon strong hybridization with the metal 3*d* states, graphene π-orbitals become magnetically polarized, which is, however, accompanied by significant changes in the electronic structure of graphene, i.e., loss of the Dirac-fermion-like character in the vicinity of the Fermi (E_F) level.[18–21] The latter problem has been tackled in two ways, either by intercalation of atomic species into existing graphene/ferromagnet interfaces in an attempt to reduce the interfacial interactions[22,23] or by realization of new interfaces with bulk ferromagnets.[24–27] However, intercalation often leads to suppression of graphene's magnetism owing to the substantial reduction of coupling to the ferromagnet,[22,23] whereas realization of novel interfaces often requires *ex situ* transfer methods,[24,25,27] which cannot guarantee the required interface purity. Recently, a particularly appealing system shifted into the focus of the studies - the epitaxial graphene/ferromagnetic Mn_5Ge_3 interface.[28] Systematic density functional theory (DFT) calculations for this system demonstrated that upon interaction with highly spin-polarized Mn_5Ge_3[29] substantial exchange splitting of the graphene π-states is induced. In particular the presence of only spin-up graphene electrons at the *K* point and at E_F, which conserve the Dirac-electron-like character, was found.[28] Following the latter theoretical assessment, experimental realization was reported, focussing on the investigation of the occupied states of the graphene/Mn_5Ge_3 interface by means of angle-resolved photoemission spectroscopy (ARPES).[30] The observed discrepancy between the experimentally measured electronic band structure and the reported DFT results,[28] was

V. Enenkel, V. Yastrebova, M. Fonin
Department of Physics
University of Konstanz
78457 Konstanz, Germany
E-mail: mikhail.fonin@uni-konstanz.de
E. Voloshina
Ruđer Bošković Institute
Division of Theoretical Physics
Bijenička cesta 54, 10000 Zagreb, Croatia
Y. Dedkov
Center for Advanced Laser Techniques
Institute of Physics
Bijenička cesta 46, 10000 Zagreb, Croatia

The ORCID identification number(s) for the author(s) of this article can be found under https://doi.org/10.1002/aelm.202500376

DOI: 10.1002/aelm.202500376

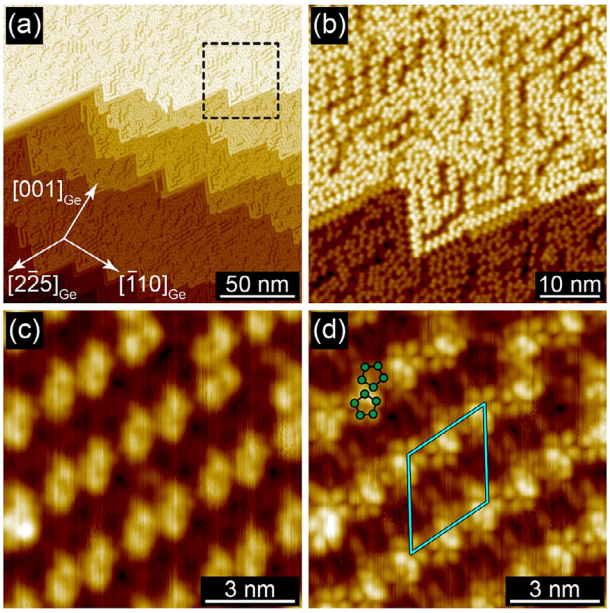

Figure 1. a) Large-scale STM image of the clean Ge(110) surface. b) Zoom on the area marked by dashed square in (a), showing the zigzag structure typical for the Ge(110)-$c(8\times10)$ surface reconstruction (both images: $V=+2$ V; $I=100$ pA; $T=4.8$ K). c) and d) High-resolution STM images of the $c(8\times10)$ structure at bias voltages +1.5 V and +1 V, respectively ($I=100$ pA (c); $I=500$ pA (d); $T=6.5$ K). Pentagon-pentagon pairs constituting the surface zigzag chain structures are visible. Unit cell (cyan rhombus) as well as two neighboring atomic pentagons (green points) are depicted in (d).

attributed to deviations in the details of the atomic interface structure, which can be experimentally addressed by local probe techniques.

In the present study, atomic structure and local electronic properties of graphene on $Mn_5Ge_3(11\bar{2}0)$ and $Mn_5Ge_3(0001)$ surfaces were investigated by means of low-temperature scanning tunneling microscopy and spectroscopy (STM and STS). These interfaces were realized by on-surface precipitation performed by annealing during and after Mn deposition on graphene/Ge(110). We analyzed the quasiparticle scattering on graphene to obtain a detailed insight into graphene's electronic structure in the vicinity of the Fermi level. The experimentally obtained energy dispersion of the charge carriers in graphene provide information about the graphene-Mn_5Ge_3 interaction.

2. Results and Discussion

Prior to graphene growth the quality and atomic structure of the Ge(110) surface was investigated by scanning tunneling microscopy (STM). **Figure 1** shows STM images of the clean Ge(110) surface. Wide monoatomic terraces of ~50–100 nm demonstrating characteristic zigzag chains are observed (Figure 1 a,b). The latter are usually attributed to the $c(8\times10)$-reconstruction formed by five-membered Ge clusters building up zigzag chains along the [2$\bar{2}$5] direction on the flat Ge(110) surface.[31–33] This reconstruction is associated with rapid cooling following high-temperature annealing, which is part of our cleaning procedure.[33] The unit element of a zigzag chain consists of a tetramer (two pairs) of such distorted Ge clusters, which are visible as bright protrusions in STM (Figure 1c). Depending on the bias voltage and tip state, Ge adatoms within the five-membered clusters can be resolved as shown in Figure 1d. Based on the thorough STM imaging of the sample surface (see also the corresponding low energy electron diffraction (LEED) images in Figure S1, Supporting Information) we conclude that the overall cleanliness and quality of the prepared Ge(110) samples correspond to that reported in earlier studies.[34,35]

The growth of graphene on Ge(110) was performed by using an atomic carbon source. The substrate temperature was kept at 925°C during carbon deposition in order to assure single domain graphene growth on Ge(110).[35–41] The growth process was stopped at a submonolayer coverage, thus, producing a sample with both graphene-covered and graphene-free areas, optimal for further Mn_5Ge_3 growth experiments.

Figure 2 a shows an overview STM topographic image of the graphene/Ge(110) surface. Flat graphene flakes with lateral sizes of up to 40 × 40 nm^2 are spread over the Ge(110) surface (see Figure 2b) achieving the cumulative coverage of about 0.3 monolayer (ML). As expected for graphene growth temperatures close to the melting point of Ge, single domain orientation is observed with the graphene armchair direction being parallel to the [$\bar{1}$10] direction of Ge(110) as can be deduced from the atomically resolved STM images. Depending on the tip state and at a sufficiently large bias voltage (both polarities), Ge underneath graphene can be resolved. The previously discussed surface reconstruction is no longer visible and the Ge atoms are now roughly aligned in rows along the [$\bar{1}$10] direction (as reported in ref. [42], see inset Figure 2b).

In order to access the local electronic properties of graphene, large-scale atomically resolved dI/dV maps were recorded on top of graphene islands (see the example given in Figure 2d). In both, STM images and dI/dV maps, the characteristic modulations of the local density of states (LDOS) due to quasiparticle interference (QPI) are observed. A 2D Fast Fourier transform (FFT) image (Figure 2e) obtained from the dI/dV map (Figure 2d) shows small round features centered at the $(\sqrt{3}\times\sqrt{3})R30°$ positions with respect to the graphene atomic lattice spots, corresponding to *intervalley* scattering. The analysis of the scattering features' sizes from the dI/dV maps recorded at different bias voltages yields the information on the scattering vectors, which is used to plot the dispersion relation $E(k)$ of graphene in the vicinity of the Fermi level (Figure 2f). The obtained data points are confined to a line, which can be fitted by $E(k)=\hbar v_F k+E_D$ yielding a Dirac point position of $E_D=(+5\pm35)$ meV with respect to E_F and a Fermi velocity of $v_F=(1.58\pm0.35)\times10^6$ m/s. Thus, our data suggests that graphene on Ge(110) is only slightly n-doped, which is in line with earlier reports, where the electronic properties of graphene/Ge(110) were studied either by angle-resolved photoelectron spectroscopy[30,42] or by STM.[35]

In the next step, nominally 40–50 MLs Mn were deposited on the graphene/Ge(110) sample kept at 450°C to induce the formation of the Mn_5Ge_3 alloy on Ge(110). **Figure 3** a represents a large scale overview STM image of the surface after Mn deposition. The surface morphology is mostly dominated by large 3D islands of two different types. The islands of the first type are triangular-prism- or wedge-shaped (bottom part of Figure 3a), whereas the islands of the second (predominant) type

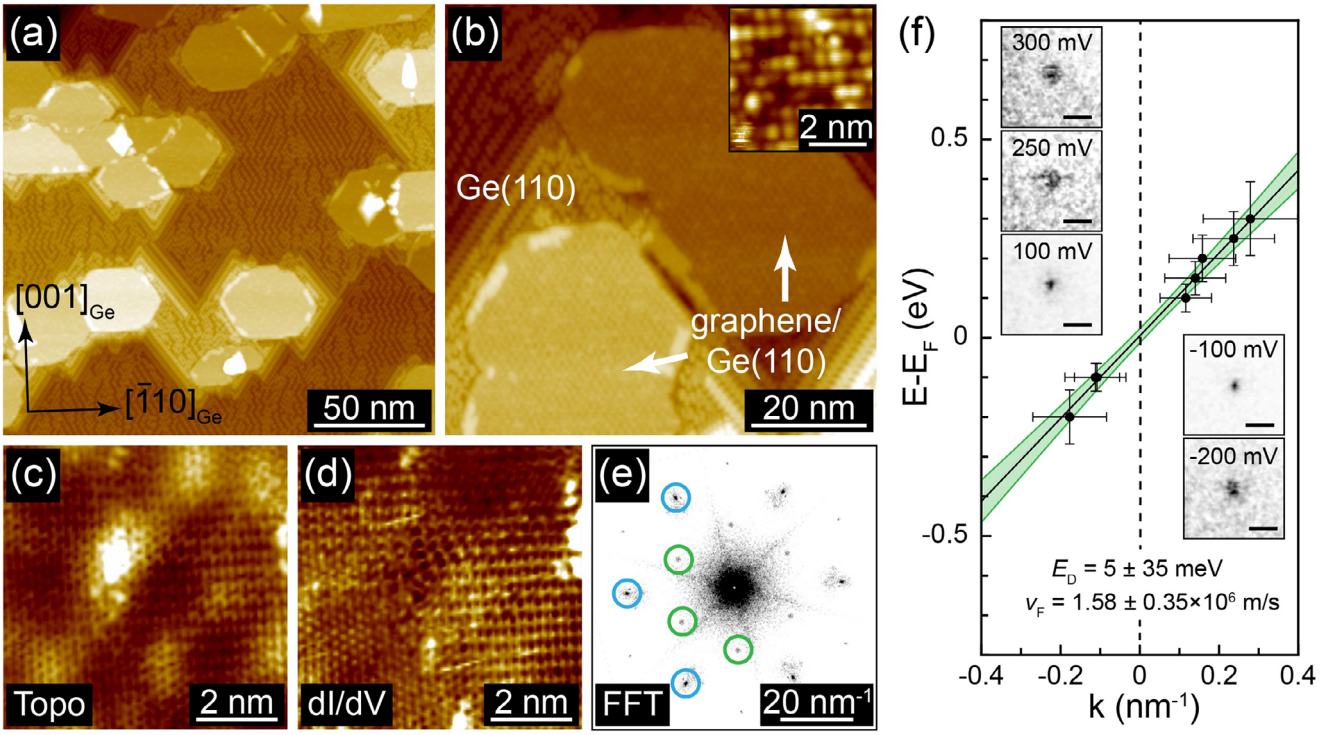

Figure 2. a) Large-scale STM topographic image of the graphene/Ge(110) sample, showing graphene flakes on top of the Ge(110) surface ($V = +2$ V; $I =$ 60 pA; $T = 4.6$ K). b) High resolution STM topography of two neighboring graphene flakes ($V = +2$ V; $I = 60$ pA; $T = 4.6$ K). Inset shows the arrangement of Ge atoms underneath graphene ($V = -2$ V; $I = 400$ pA; $T = 4.6$ K). c) Atomically resolved STM topography obtained on top of a graphene flake on the Ge(110) surface ($V = +0.3$ V; $I = 400$ pA; $V_{mod} = 110$ mV; $T = 4.6$ K). d) Simultaneously recorded dI/dV map of the area shown in (c) showing LDOS modulations due to charge carrier scattering. e) 2D FFT image of the map presented in (d) showing graphene atomic lattice spots (marked by blue circles) as well as *intervalley* scattering features located at the $(\sqrt{3} \times \sqrt{3})R30°$ positions (marked by green circles). f) Electronic dispersion relation $E(k)$ of the graphene flake shown in (c) and (d), as derived from the size of *intervalley* scattering features obtained from dI/dV maps recorded at different bias voltages (44.2×21.5 nm^2; $I = 400$ pA; $T = 4.6$ K). The corresponding fit is shown as a solid line. Confidence interval is shown in green. Insets: Magnifications of the *intervalley* scattering features at various energies (scale bars in all FFTs: 2 nm^{-1}). All presented FFT images are symmetrized for clarity by rotating the FFT by 60° and 120°, then overlaying the original and both rotated images and thereby adding up their intensities.

show a rectangular shape with a flat plateau on top (upper part of Figure 3a).

Figure 3b,d shows high-resolution STM images obtained on one of the faces of a wegde-shaped island presented in Figure 3a. The atomically-resolved image shows a honeycomb structure with a periodicity of about 7.2 Å (obtained from the analysis of STM (Figure 3d) and the corresponding Fast Fourier transform (Figure 3e) images) being very close to the unit cell parameter $a = 7.184$ Å of Mn_5Ge_3 suggesting the formation of the $Mn_5Ge_3(0001)$ surface.

The honeycomb structure contrast is consistent with the Mn-termination on top of Mn_5Ge_3.[43–46] The corresponding atomic model is presented in Figure 3 d with Mn surface layer atoms marked as Mn-(S). The step height between two adjacent terraces of the $Mn_5Ge_3(0001)$ nanoisland obtained from the height profile (bottom panel of Figure 3b), amounts to about 5 Å being very close to the unit cell parameter of $c = 5.053$ Å.

Figure 3c,f shows high-resolution STM images obtained on top of a rectangular island. The analysis of the symmetry and lattice parameters obtained from atomically-resolved STM images (Figure 3f) and corresponding 2D FFT images (Figure 3g) yield a rectangular lattice with parameters of about $a = 5.1$ Å and $b = 12.5$ Å. This is consistent with the $(11\bar{2}0)$ surface plane of the Mn_5Ge_3 crystal (unit cell parameters are $a = 5.053$ Å and $b = 12.443$ Å). The atomic model of the Mn-terminated $Mn_5Ge_3(11\bar{2}0)$ surface is shown in Figure 3f. The atomic rows visible in the STM image correspond to the two-atom Mn rows running along the [0001]-direction. Every single feature within the row correspond to two pairs of surface Mn atoms constituting a rectangle with a second layer Ge atom in the center. The step height of about 3.5 Å between the adjacent terraces corresponds to the interlayer distance $d = 3.592$ Å along the $[11\bar{2}0]$ direction. The epitaxial orientations of the two types of islands with respect to the substrate correspond to $Mn_5Ge_3(11\bar{2}0)||Ge(110)$ with $[11\bar{2}0]_{Mn_5Ge_3} \parallel [110]_{Ge}$; $[\bar{1}100]_{Mn_5Ge_3} \parallel [\bar{1}10]_{Ge}$ and $Mn_5Ge_3(0001)$ roughly parallel to Ge(001) with $[0001]_{Mn_5Ge_3}$ roughly parallel to $[001]_{Ge}$.[45]

Upon Mn_5Ge_3 formation, intercalation of Mn in the graphene/Ge(110) interface takes place, which leads to the presence of graphene flakes on top of the Mn_5Ge_3 islands. Graphene flakes can be easily distinguished owing to their particular shape on top of Mn_5Ge_3 islands observed in STM images, as shown in Figure 3, and do not change in size or distribution compared to the initial coverage on Ge(110). Graphene flakes are found on terraces away from step edges (Figure 3a) or partially incorporated into Mn_5Ge_3 terraces with the flake edge being

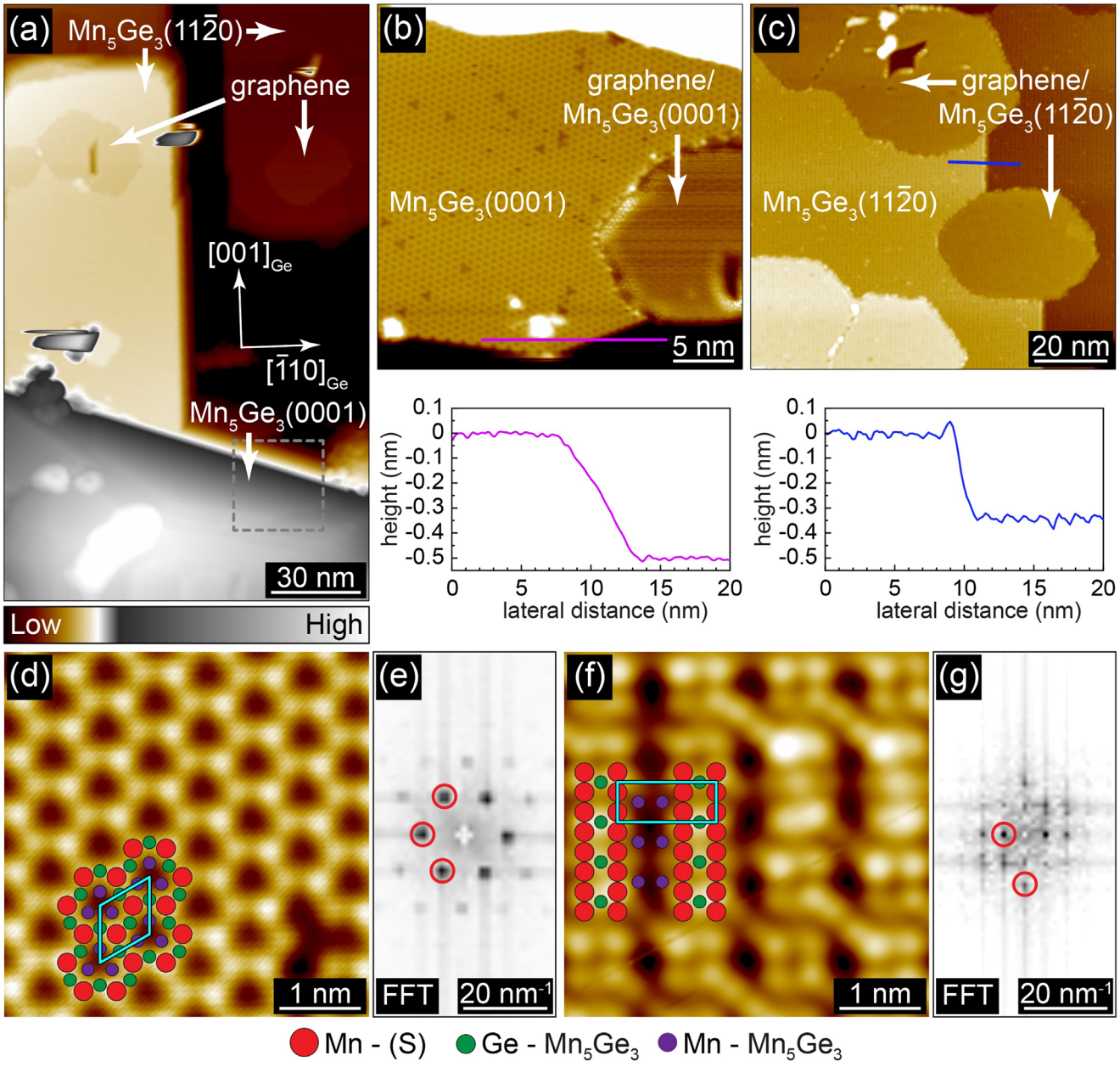

Figure 3. a) Large-scale STM topographic image of the surface after Mn deposition showing compact Mn_5Ge_3 islands ($V = +1.3$ V; $I = 60$ pA, $T = 4.6$ K). b) STM image obtained on top of a $Mn_5Ge_3(0001)$ island (marked by dashed square in (a)) together with the corresponding height profile ($V = +1$ V; $I = 700$ pA; $T = 4.6$ K). c) STM image obtained on top of a $Mn_5Ge_3(11\bar{2}0)$ island together with the corresponding height profile ($V = +2$ V; $I = 60$ pA; $T = 4.6$ K). Both islands show graphene flakes on top. d) Atomically-resolved STM image of the $Mn_5Ge_3(0001)$ surface ($V = -200$ mV; $I = 700$ pA; $T = 5.7$ K). Corresponding unit cell (cyan rhombus) and atomic model are depicted. e) 2D FFT image of (d) with the reciprocal lattice spots of $Mn_5Ge_3(0001)$ marked by red circles. f) Atomically-resolved STM image of the $Mn_5Ge_3(11\bar{2}0)$ surface ($V = +10$ mV; $I = 100$ pA; $T = 5.7$ K). Corresponding unit cell (cyan rectangle) and atomic model are depicted. g) 2D FFT image of (f) with the reciprocal lattice spots of $Mn_5Ge_3(11\bar{2}0)$ marked by red circles.

connected to the adjacent Mn_5Ge_3 step-edge (Figure 3b,c). The flakes' surface appears very flat with only very small corrugation. Depending on the applied bias voltage and tip state we are able to discriminate between the Mn_5Ge_3 and graphene surface areas. For suitable tip states and often larger bias voltages (both polarities) graphene is virtually transparent. Only flake contours as well as an unaltered atomic structure of Mn_5Ge_3 underneath the graphene layer are visible, in contrast to the altered atomic structure of Ge(110) discussed earlier. When the bias voltage is lowered toward E_F, the atomic lattice of graphene can be resolved, as shown in **Figure 4a,b** on top of $Mn_5Ge_3(0001)$ and $Mn_5Ge_3(11\bar{2}0)$, respectively.

2D FFT images obtained from the STM topographies show the presence of both graphene-related and Mn_5Ge_3-related atomic spots (Figure 4c,d) and allow for the identification of the graphene lattice orientation with respect to the underlying

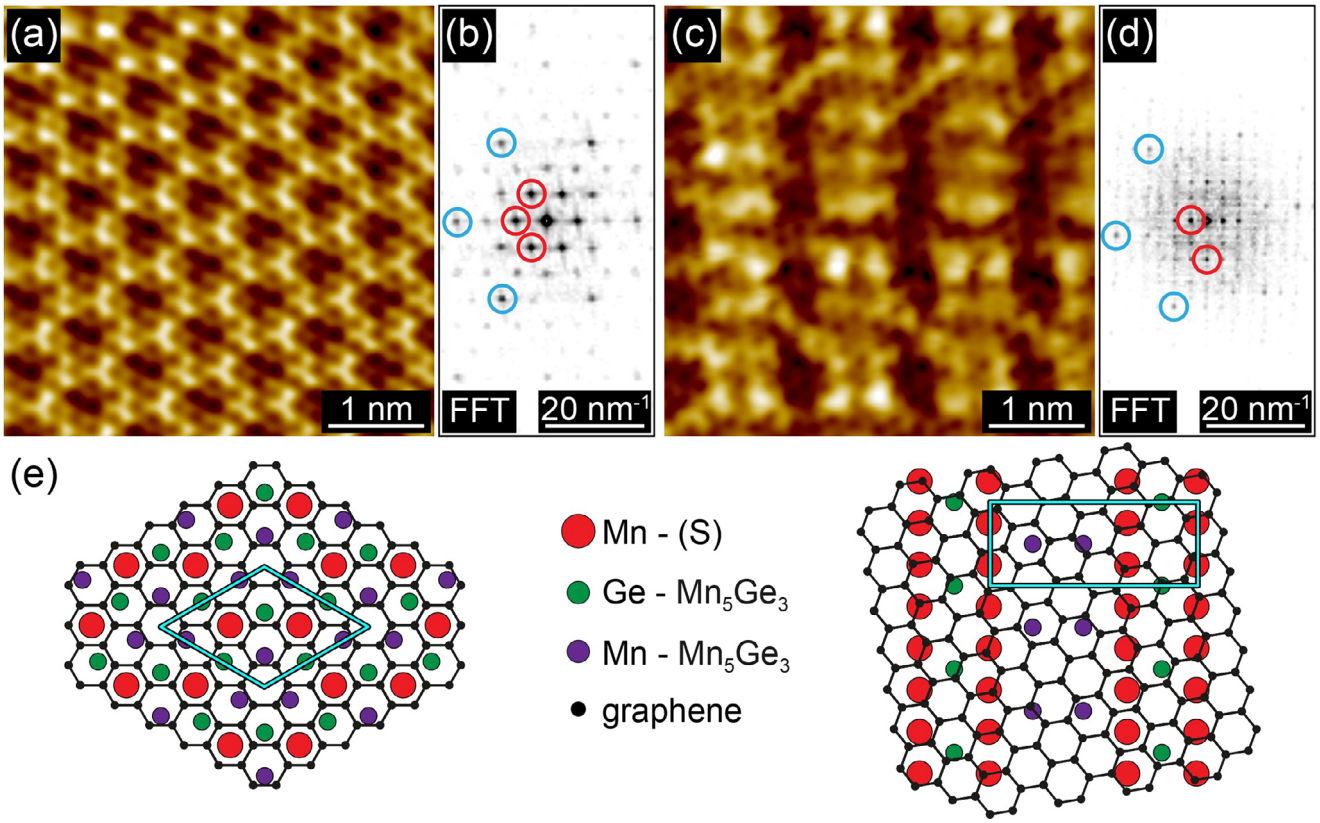

Figure 4. a) and c) Atomically-resolved STM images of graphene on Mn_5Ge_3(0001) and on $Mn_5Ge_3(11\bar{2}0)$, respectively ((a): $V = -200$ mV; $I = 700$ pA, $T = 4.6$ K, (c) $V = -10$ mV; $I = 100$ pA, $T = 4.6$ K). b) and d) 2D FFT images obtained from (a) and (c), respectively. Graphene reciprocal lattice spots are marked by blue circles, Mn_5Ge_3 atomic lattice spots are marked by red circles. e) Top views of the atomic ball models of graphene/Mn_5Ge_3(0001) and graphene/$Mn_5Ge_3(11\bar{2}0)$, respectively. The cyan rhombus and the cyan rectangle correspond to the Mn_5Ge_3 unit cells.

substrate lattice. For the graphene/Mn_5Ge_3(0001) interface we found that graphene is aligned to the substrate with the graphene zigzag edges along the Mn_5Ge_3 $[\bar{1}010]$ and the armchair edges along Mn_5Ge_3 $[\bar{1}2\bar{1}0]$ directions. The lattice arrangement roughly corresponds to a (3 × 3) graphene/Mn_5Ge_3(0001) structure, as presented in Figure 4b (bottom panel) as an atomic model. In case of graphene/$Mn_5Ge_3(11\bar{2}0)$ the situation turns out to be more complex as the honeycomb graphene lattice has to accommodate the rectangular atomic lattice of the substrate. Graphene zigzag edges are found to align roughly along the Mn_5Ge_3 [0001] and the armchair edges along $Mn_5Ge_3[\bar{1}100]$ directions, as presented in the atomic model in Figure 4d (bottom panel). We note that, as for graphene/Ge(110), small rotational offsets of up to 9° relative to these directions can be found depending on the actual graphene flake, (see also the corresponding low energy electron diffraction (LEED) images in Figure S1, Supporting Information). The exact origin of these small rotational offsets[37,39] remains unclear. One possible explanation is that, despite temperatures being within a few degrees of the Ge melting point, they may still be insufficient to completely anneal out orientation defects. Alternatively, the weak interaction between graphene and the Ge(110) surface, may allow for a small degree of rotational freedom during nucleation and growth. Overall, our STM results indicate the formation of clean and flat graphene/Mn_5Ge_3 interfaces with a high degree of structural order down to the atomic level within the investigated regions.

In order to obtain information about the electronic properties of graphene/Mn_5Ge_3, QPI (dI/dV) maps were recorded on extended graphene flakes on flat Mn_5Ge_3 terraces. We note that a pronounced scattering in graphene on Mn_5Ge_3 could be observed, which allows for dI/dV map sizes down to about 10 × 10 nm^2, thus, providing enough intensity in QPI as well as acquisition of dI/dV maps in a very broad voltage range between −700 mV and +900 mV. **Figure 5**a,b shows examples of dI/dV maps together with the corresponding 2D FFT images. Besides the atomic spots, we observe *intervalley* scattering features centered at the $(\sqrt{3} \times \sqrt{3})R30°$ positions with respect to the graphene atomic lattice spots.

As shown in Figure 5d, the overall round intervalley scattering features clearly vary in size with energy. While they appear point-like close to E_F (between ±300 mV), at energies further away they gradually open into a circle, for both occupied and unoccupied states. Even at energies particularly close to E_F, e.g., ±2 mV, scattering in graphene is still observed (see Figure S2, Supporting Information) setting the margin of a possible band gap size to just several millielectronvolt. Recent ARPES results[30] indicated the existence of a bandgap of 20±10 meV, being somewhat larger as observed in our studies. This can be explained by averaging over different adsorption configurations and thus

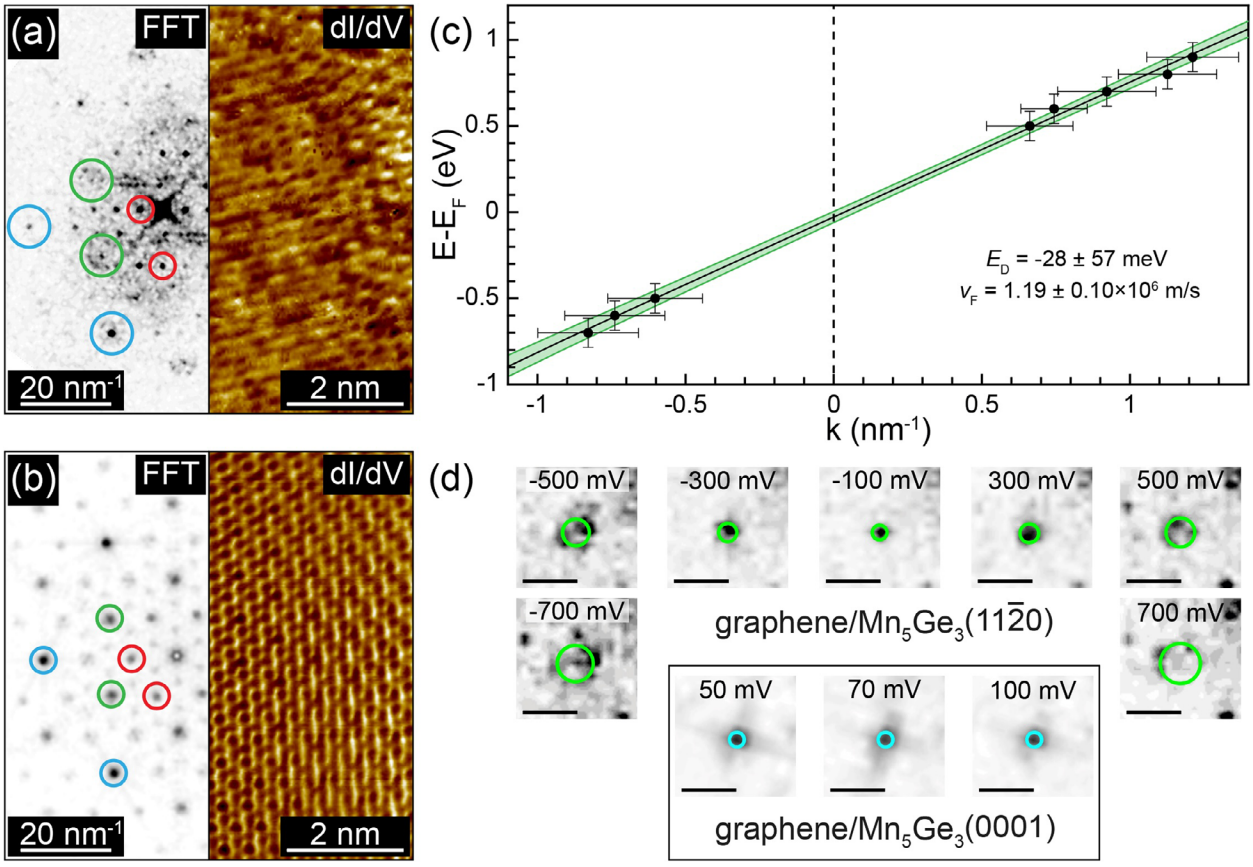

Figure 5. a) and b) Atomically-resolved dI/dV maps and corresponding FFT images of the graphene/Mn_5Ge_3(11$\bar{2}$0) and graphene/Mn_5Ge_3(0001) surfaces, respectively ((a): $V = +900$ mV; $I = 700$ pA; $V_{mod} = 100$ mV; $T = 4.6$ K; (b): $V = +50$ mV; $I = 500$ pA; $V_{mod} = 20$ mV; $T = 5.4$ K). In FFT images the features are marked as follows: graphene reciprocal lattice - blue, *intervalley* scattering features - green, Mn_5Ge_3 reciprocal lattice - red. c) Electronic dispersion relation $E(k)$ of graphene/Mn_5Ge_3(11$\bar{2}$0), as derived from the size of *intervalley* scattering features obtained from dI/dV maps recorded at different bias voltages. The corresponding fit is shown as a solid line. Confidence interval is shown in green. d) Magnifications of the *intervalley* scattering features at various energies obtained on graphene/Mn_5Ge_3(11$\bar{2}$0) (scale bars in all FFTs: 5nm^{-1}; maps: 10.4 × 10.4 nm^2; $I = 700$ pA; $T = 4.6$ K) as well as on graphene/Mn_5Ge_3(0001) (scale bars in all FFTs: 5nm^{-1}; maps: 7.8 × 7.8 nm^2; $I = 500$ pA; $T = 5.4$ K). FFT images of graphene/Mn_5Ge_3(0001) are symmetrized. All features are marked by circles as guide for the eye. We note that at energies further away from the Dirac point trigonal warping sets in and the features are not exactly round any more. For the energies with noticeable warping the measured values correspond to the Γ-*K* direction, which exhibits linear dispersion in the relevant energy range.

different average interaction strength between graphene and Mn_5Ge_3 in case of ARPES compared to the local measurement presented in our work. The analysis of the QP scattering features from the maps obtained on graphene/Mn_5Ge_3(11$\bar{2}$0) at different energies allow us to plot the dispersion relation $E(k)$ of graphene (Figure 2c). The experimental data yields a linear dispersion relation for graphene with $E_D = (-28 \pm 57)$ meV with respect to E_F and a Fermi velocity of $v_F = (1.19 \pm 0.1) \times 10^6$ m/s. For graphene/Mn_5Ge_3(0001) only few dI/dV maps around E_F could be acquired showing only point-like *intervalley* scattering features (see Figure 5d), which could not be used for the quantitative dispersion analysis but suggesting that the position of the Dirac point is also close to E_F as found for graphene/Mn_5Ge_3(11$\bar{2}$0). **Table 1** summarizes the different values of E_D and v_F obtained in this study.

We further investigated the electronic properties of graphene by single-point dI/dV spectroscopy. **Figure 6** shows a single-point dI/dV spectrum recorded on graphene/Ge(110) (violet) showing three pronounced features at bias voltages of –1 V, –0.55 V, and +0.8 V. Those dominant features stem from the surface states of Ge(110) underneath graphene as discussed in earlier studies,[47,48] thus, suggesting only a small influence of graphene on the observed DOS. Further spectroscopic measurements were performed on Mn_5Ge_3(0001) as well as graphene/Mn_5Ge_3(0001), which are also shown in Figure 6. These area-averaged dI/dV curves show a metallic character and overall comparable spectral shape, which does not show

Table 1. Summary of Dirac point energies (E_D) and Fermi velocities (v_F) for the different studied systems.

System	E_D [meV]	v_F [× 10^6 m/s]
Graphene/Ge(110)	+5±35	1.58±0.35
Graphene/Mn_5Ge_3(11$\bar{2}$0)	−28±57	1.19±0.1

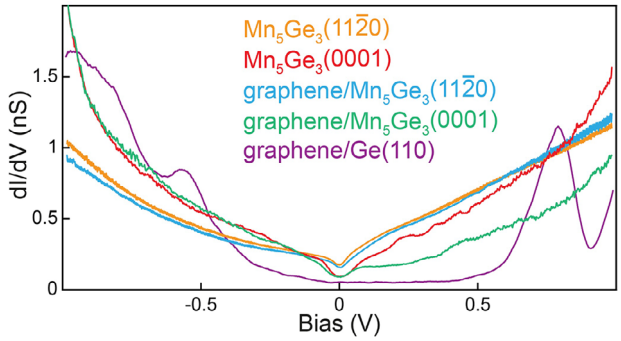

Figure 6. Single-point dI/dV spectrum obtained on graphene/Ge(110) – violet (V_{set} = 1 V; I = 300 pA; T = 4.6 K). Area-averaged dI/dV spectra (5 × 5 point grid on 5 × 5 nm^2; V_{set} = –1 V; I = 700 pA; T = 4.6 K) obtained on Mn_5Ge_3(11$\bar{2}$0) – orange, graphene/Mn_5Ge_3(11$\bar{2}$0) – blue, Mn_5Ge_3(0001) – red and graphene/Mn_5Ge_3(0001) – green.

particularly pronounced features in the range between –1 and +1 V. Only small variations of DOS are visible, which can be attributed to the presence of surface/interface states.[28,46] The small dip at E_F most likely originates from spin-splitting of the Mn_5Ge_3 bands, resulting in a reduction of the total DOS at E_F.[28] For Mn_5Ge_3(11$\bar{2}$0) and graphene/Mn_5Ge_3(11$\bar{2}$0) the spectra show roughly the same shape as for the case of the (0001) plane. No features pointing at strong hybridization between the electronic states of Mn_5Ge_3 and graphene π-bands are observed, thus suggesting a decoupled quasi-free-standing graphene layer, which is in agreement with our dI/dV mapping results.

Thus, our data points at the realization of the graphene/Mn_5Ge_3 interface with graphene being particularly close to charge neutrality and the value of v_F almost coinciding with that of free-standing graphene. The formation of quasi-free-standing graphene can be attributed to the absence of orbital mixing of the electronic states of graphene and Mn_5Ge_3 close to the Fermi level, which can be deduced from the analysis based on the DFT calculations.[28] Our findings are in line with recent ARPES experiments,[30] where linear dispersion of the graphene-derived π-bands around the K-point and a small n-doping was observed upon Mn intercalation underneath graphene on Ge and formation of graphene/Mn_5Ge_3. In particular, a very good agreement with our study is found for the extracted positions of the Dirac points $E_D - E_F$ = (–65 ± 10) meV for graphene/Mn_5Ge_3/Ge(110) and $E_D - E_F$ = (–90 ± 10) meV for graphene/Mn_5Ge_3/Ge(111), respectively.

3. Conlusion

We performed a detailed study of the atomic structure and local electronic properties of the epitaxial graphene/Mn_5Ge_3/Ge(110) system prepared by Mn evaporation on graphene/Ge(110) combined with annealing during and after deposition. Mn_5Ge_3 crystallites of two different types, each showing a primary plane of Mn_5Ge_3 – Mn_5Ge_3(0001) and Mn_5Ge_3(11$\bar{2}$0) – are found on the sample surface after the solid-state precipitation. Low-temperature STM studies show graphene/Mn_5Ge_3 interfaces for both types of crystallographic structures very well ordered down to the atomic level within the investigated regions. The local electronic structure of graphene/Mn_5Ge_3 was thoroughly characterized by quasiparticle interference mapping and single-point dI/dV spectroscopy. Graphene is characterized by the linear dispersion of the π– bands around the K point with a Fermi velocity of v_F = 1.19 ± 0.1 × 10^6 m/s and a particularly small n-doping of $E_D - E_F$ = –28 ±57 meV. The quasi-free-standing nature of graphene on Mn_5Ge_3 is explained by the rather weak orbital mixing of the electronic states of Mn_5Ge_3 and graphene π-bands close to the Fermi level. Taking into account the strong exchange-splitting in ferromagnetic Mn_5Ge_3, proximity exchange of Dirac electrons in graphene/Mn_5Ge_3 can still be present even without strong orbital hybridization in the vicinity of the Dirac point, thus, encouraging further investigations of this interface with the main focus on spin-resolved experiments regarding graphene π-states.

4. Experimental Section

Growth and STM studies were performed in a ultra-high vacuum system (Scienta Omicron) with base pressure of 1 × 10^{-10} mbar. Ge(110) substrates (G-materials (Germany), Sb-doped, resistivity 0.015 –0.017 Ω·cm) were cleaned by repeated cycles of Ar$^+$-sputtering (1.5 keV; p_{Ar} = 5.5 × 10^{-5} mbar) and subsequent annealing (T = 870°C). Graphene was grown by carbon evaporation from an atomic carbon source (Dr. Eberl MBE-Komponenten GmbH) with the substrate temperature kept at T = 925°C. Mn evaporation was performed from an effusion cell (Dr. Eberl MBE-Komponenten GmbH) at a fixed rate of 2 Å/min onto the graphene/Ge(110) sample kept at 450°C. This procedure yields large epitaxial Mn_5Ge_3 islands on Ge(110). The temperature was chosen based on previous studies demonstrating efficient formation of Mn_5Ge_3 on Ge(111)[29,43,44,46] and Ge(001)[45] by annealing after Mn deposition in the temperature range of 300–650°C. Low-temperature STM experiments were performed in a Cryogenic STM (Scienta Omicron) operated at 4-10 K. STM data were acquired in the constant-current mode using grinded and polished PtIr tips (Nanoscore GmbH). The sign of the bias voltage (V) corresponded to the potential applied to the sample. The differential conductance dI/dV point spectra as well as dI/dV mappings were acquired using a standard lock-in technique or by numerical differentiation of the I–V curves, with parameters given in the paper text.

Supporting Information

Supporting Information is available from the Wiley Online Library or from the author.

Acknowledgements

This work was financially supported the Deutsche Forschungsgemeinschaft (DFG) - FO 640/8-1. Y.D. acknowledges the support by the project Centre for Advanced Laser Techniques (CALT), co-funded by the European Union through the European Regional Development Fund under the Competitiveness and Cohesion Operational Programme (Grant No. KK.01.1.1.05.0001). E.V. acknowledges the support by the European Union's NextGenerationEU program.

Conflict of Interest

The authors declare no conflict of interest.

Data Availability Statement

The data that support the findings of this study are available from the corresponding author upon reasonable request.

Keywords

Ge(110), graphene, Mn_5Ge_3, quasiparticle interference mapping, scanning tunneling microscopy

Received: June 4, 2025
Revised: September 10, 2025
Published online: October 21, 2025

[1] K. S. Novoselov, A. K. Geim, S. V. Morozov, D. Jiang, Y. Zhang, S. V. Dubonos, I. V. Grigorieva, A. A. Firsov, *Science* **2004**, *306*, 666.
[2] K. S. Novoselov, A. K. Geim, S. V. Morozov, D. Jiang, M. I. Katsnelson, I. V. Grigorieva, S. V. Dubonos, A. A. Firsov, *Nature* **2005**, *438*, 197.
[3] Y. Zhang, Y. W. Tan, H. L. Stormer, P. Kim, *Nature* **2005**, *438*, 201.
[4] A. H. Castro Neto, F. Guinea, N. M. R. Peres, K. S. Novoselov, A. K. Geim, *Rev. Mod. Phys.* **2009**, *81*, 109.
[5] A. K. Geim, *Science* **2009**, *324*, 1530.
[6] K. S. Novoselov, *Rev. Mod. Phys.* **2011**, *83*, 837.
[7] N. Tombros, C. Jozsa, M. Popinciuc, H. T. Jonkman, B. J. van Wees, *Nature* **2007**, *448*, 571.
[8] W. Han, R. K. Kawakami, M. Gmitra, J. Fabian, *Nat. Nanotechnol.* **2014**, *9*, 794.
[9] S. Roche, J. Åkerman, B. Beschoten, J.-Ch. Charlier, M. Chshiev, S. P. Dash, B. Dlubak, J. Fabian, A. Fert, M. Guimarães, F. Guinea, I. Grigorieva, C. Schönenberger, P. Seneor, C. Stampfer, S. O. Valenzuela, X. Waintal, B. van Wees, *2D Mater.* **2015**, *2*, 030202.
[10] M. V. Kamalakar, C. Groenveld, A. Dankert, S. P. Dash, *Nat. Commun.* **2015**, *6*, 6766.
[11] J.-F. Dayen, S. J. Ray, O. Karis, I. J. Vera-Marun, M. V. Kamalakar, *Appl. Phys. Rev.* **2020**, *7*, 011303.
[12] A. Avsar, H. Ochoa, F. Guinea, B. Özyilmaz, B. J. van Wees, I. J. Vera-Marun, *Rev. Mod. Phys.* **2020**, *92*, 021003.
[13] V. M. Karpan, G. Giovannetti, P. A. Khomyakov, M. Talanana, A. A. Starikov, M. Zwierzycki, J. van den Brink, G. Brocks, P. J. Kelly, *Phys. Rev. Lett.* **2007**, *99*, 176602.
[14] V. M. Karpan, P. A. Khomyakov, A. A. Starikov, G. Giovannetti, M. Zwierzycki, M. Talanana, G. Brocks, J. van den Brink, P. J. Kelly, *Phys. Rev. B* **2008**, *78*, 195419.
[15] V. M. Karpan, P. A. Khomyakov, G. Giovannetti, A. A. Starikov, P. J. Kelly, *Phys. Rev. B* **2011**, *84*, 153406.
[16] Yu. S. Dedkov, M. Fonin, C. Laubschat, *Appl. Phys. Lett.* **2008**, *92*, 052506.
[17] Yu. S. Dedkov, M. Fonin, U. Rüdiger, C. Laubschat, *Appl. Phys. Lett.* **2008**, *93*, 022509.
[18] Yu. S. Dedkov, M. Fonin, *New J. Phys.* **2010**, *12*, 125004.
[19] A. Dahal, M. Batzill, *Nanoscale* **2014**, *6*, 2548.
[20] D. Marchenko, A. Varykhalov, J. Sánchez-Barriga, O. Rader, C. Carbone, G. Bihlmayer, *Phys. Rev. B* **2015**, *91*, 235431.
[21] D. Usachov, A. Fedorov, M. M. Otrokov, A. Chikina, O. Vilkov, A. Petukhov, A. G. Rybkin, Y. M. Koroteev, E. V. Chulkov, V. K. Adamchuk, A. Grüneis, C. Laubschat, D. V. Vyalikh, *Nano Lett.* **2015**, *15*, 2396.
[22] N. I. Verbitskiy, A. V. Fedorov, G. Profeta, A. Stroppa, L. Petaccia, B. Senkovskiy, A. Nefedov, C. Wöll, D. Yu. Usachov, D. V. Vyalikh, L. V. Yashina, A. A. Eliseev, T. Pichler, A. Grüneis, *Sci. Rep.* **2015**, *5*, 17700.
[23] Yu. Dedkov, W. Klesse, A. Becker, F. Späth, C. Papp, E. Voloshina, *Carbon* **2017**, *121*, 10.
[24] Z. Wang, C. Tang, R. Sachs, Y. Barlas, J. Shi, *Phys. Rev. Lett.* **2015**, *114*, 016603.
[25] P. Wei, S. Lee, F. Lemaitre, L. Pinel, D. Cutaia, W. Cha, F. Katmis, Y. Zhu, D. Heiman, J. Hone, J. S. Moodera, C.-T. Chen, *Nat. Mater.* **2016**, *15*, 711.
[26] K. Zollner, M. Gmitra, T. Frank, J. Fabian, *Phys. Rev. B* **2016**, *94*, 155441.
[27] D. A. Solis, A. Hallal, X. Waintal, M. Chshiev, *Phys. Rev. B* **2019**, *100*, 104402.
[28] E. Voloshina, Yu. Dedkov, *J. Phys. Chem. Lett.* **2019**, *10*, 3212.
[29] Yu. S. Dedkov, M. Holder, G. Mayer, M. Fonin, A. B. Preobrajenski, *J. Appl. Phys.* **2009**, *105*, 073909.
[30] Yu. Dedkov, J. Yang, H. Hu, Y. Jin, M. Yan, Y. Jin, J. Zhou, E. Voloshina, *ACS Appl. Mater. Interfaces* **2023**, *15*, 26190.
[31] T. Ichikawa, *Surf. Sci.* **2004**, *560*, 213.
[32] T. Ichikawa, *Surf. Sci.* **2004**, *560*, 205.
[33] C. H. Mullet, S. Chiang, *Surf. Sci.* **2014**, *621*, 184.
[34] J. Tesch, E. Voloshina, M. Fonin, Yu. Dedkov, *Carbon* **2017**, *122*, 428.
[35] J. Tesch, F. Paschke, M. Fonin, M. Wietstruk, S. Böttcher, R. J. Koch, A. Bostwick, Ch. Jozwiak, E. Rotenberg, A. Makarova, B. Paulus, E. Voloshina, Yu. Dedkov, *Nanoscale* **2018**, *10*, 6088.
[36] G. Wang, M. Zhang, Y. Zhu, G. Ding, D. Jiang, Q. Guo, S. Liu, X. Xie, P. K. Chu, Z. Di, X. Wang, *Sci. Rep.* **2013**, *3*, 2465.
[37] J.-H. Lee, E. K. Lee, W.-J. Joo, Y. Jang, B.-S. Kim, J. Y. Lim, S.-H. Choi, S. J. Ahn, J. R. Ahn, M.-H. Park, C.-W. Yang, B. L. Choi, S.-W. Hwang, D. Whang, *Science* **2014**, *344*, 286.
[38] B. Kiraly, R. M. Jacobberger, A. J. Mannix, G. P. Campbell, M. J. Bedzyk, M. S. Arnold, M. C. Hersam, N. P. Guisinger, *Nano Lett.* **2015**, *15*, 7414.
[39] P. C. Rogge, M. E. Foster, J. M. Wofford, K. F. McCarty, N. C. Bartelt, O. D. Dubon, *MRS Communications* **2015**, *5*, 539.
[40] Yu. Dedkov, E. Voloshina, *Nanoscale* **2020**, *12*, 11416.
[41] L. Persichetti, M. De Seta, A. M. Scaparro, V. Miseikis, A. Notargiacomo, A. Ruocco, A. Sgarlata, M. Fanfoni, F. Fabbri, C. Coletti, L. Di Gaspare, *Appl. Surf. Sci.* **2020**, *499*, 143923.
[42] M. Galbiati, L. Persichetti, P. Gori, O. Pulci, M. Bianchi, L. Di Gaspare, J. Tersoff, C. Coletti, P. Hofmann, M. De Seta, L. Camilli, *J. Phys. Chem. Lett.* **2021**, *12*, 1262.
[43] C. Zeng, S. C. Erwin, L. C. Feldman, A. P. Li, R. Jin, Y. Song, J. R. Thompson, H. H. Weitering, *Appl. Phys. Lett.* **2003**, *83*, 5002.
[44] C. Zeng, W. Zhu, S. C. Erwin, Z. Zhang, H. H. Weitering, *Phys. Rev. B* **2004**, *70*, 205340.
[45] H. Kim, G.-E. Jung, J.-H. Lim, K. H. Chung, S.-J. Kahng, W.-j. Son, S. Han, *Nanotechnology* **2008**, *19*, 025707.
[46] J. H. Grytzelius, H. M. Zhang, L. S. O. Johansson, *Phys. Rev. B* **2011**, *84*, 195306.
[47] P. Bampoulis, A. Acun, L. Zhang, H. J. W. Zandvliet, *Surf. Sci.* **2014**, *626*, 1.
[48] H. W. Kim, W. Ko, W.-J. Joo, Y. Cho, Y. Oh, J. Y. Ku, I. Jeon, S. Park, S. W. Hwang, *J. Phys. Chem. Lett.* **2018**, *9*, 7059.